eTransportation 16 (2023) 100231

Contents lists available at ScienceDirect

eTransportation

journal homepage: www.journals.elsevier.com/etransportation

Investigating re-parametrization of electrochemical model-based battery management using real-world driving data

Moritz Streb [a,*,1], Malin Andersson [b,c,1], Verena Löfqvist Klass [c], Matilda Klett [a,c], Mikael Johansson [b], Göran Lindbergh [a]

[a] Applied Electrochemistry, Department of Chemical Engineering, School of Engineering Sciences in Chemistry, Biotechnology and Health, KTH Royal Institute of Technology, 100 44 Stockholm, Sweden

[b] Division of Decision and Control Systems, Department of Intelligent Systems, School of Electrical Engineering and Computer Science, KTH Royal Institute of Technology, 100 44 Stockholm, Sweden

[c] Scania CV, Granparksvägen 10, 151 48 Södertälje, Sweden

ARTICLE INFO

Keywords:
Battery management system
Electrochemical control
Sensitivity analysis
Battery parametrization
Heavy-duty electric vehicles

ABSTRACT

Li-ion batteries in electric vehicles must be utilized more efficiently to lower their economic and environmental cost. To achieve this increase in efficiency, it is of large interest to develop more thorough battery management that can predict internal states in online settings and update usage and control accordingly. Electrochemical models are an important tool in achieving this, and their implementation in battery management systems is the topic of ongoing research. However, electrochemical battery management relies on accurate parametrization and thus requires re-parametrization as a battery ages. We therefore studied viability of re-parametrization for electrochemical model-based battery management. To this end, we performed global sensitivity analysis on selected Doyle–Fuller–Newman model parameters using on-board current measurements. Representative driving data was collected from several types of heavy-duty vehicles. This elucidated which model parameters should be updated periodically to conserve model accuracy and which parameters are sensitive enough to be estimated from the on-board data. Additionally, we studied how parameter uncertainty affects estimation of internal states and highlight how model-based state estimation relying on a beginning-of-life parametrization degrades as electrochemical parameters change with aging.

1. Introduction

Electrification of transport systems can play a key role in combating climate change [1] and lithium-ion battery powered electric vehicles (EVs) are at the forefront of this transition [2]. The first generation of EVs emerging on the market were passenger cars but in recent years, electrification efforts also involve the heavy-duty vehicle sector. This places increased demands on lithium-ion battery systems since heavy-duty vehicles have greater weight, more diverse use-cases and higher up-time compared to passenger cars [3]. Monitoring and control of lithium-ion batteries on-board EVs is essential for achieving safe operation, a high degree of utilization and long lifetime [4]. Conventional battery management systems (BMS) attempt these tasks using measurements of input current, output voltage and temperature together with empirical models. However, these approaches offer limited physical insight into battery-internal states. Advanced BMS therefore increasingly use electrochemical models that can map input–output data to physical states [5]. Extensive parametrization and characterization is performed in beginning-of-life (BOL) to achieve high accuracy. However, model parameters change as a battery ages which deteriorates model performance [6–9]. A sensitivity analysis (SA) can quantify the impact of parameter uncertainty on model output and indicate parameter identifiability from data [10]. In this work, we therefore performed SA of the parameters of an electrochemical battery model to study the possibility, and necessity, for re-parametrization from on-board measurements.

Several authors have studied electrochemical models for battery management [8,11–17], e.g. to limit lithium-plating during fast charging [16] or estimate the state-of-charge (SOC) [13], state-of-health (SOH) [8] and available power [12] during operation. All these approaches require accurate models to be reliable. This is a challenge in EVs, since the internal battery parameters change with aging but the on-board setting prevents conventional model parametrization methods

* Corresponding author.
E-mail address: streb@kth.se (M. Streb).
[1] These authors contributed equally.

https://doi.org/10.1016/j.etran.2023.100231
Received 21 September 2022; Received in revised form 27 January 2023; Accepted 8 February 2023
Available online 11 February 2023

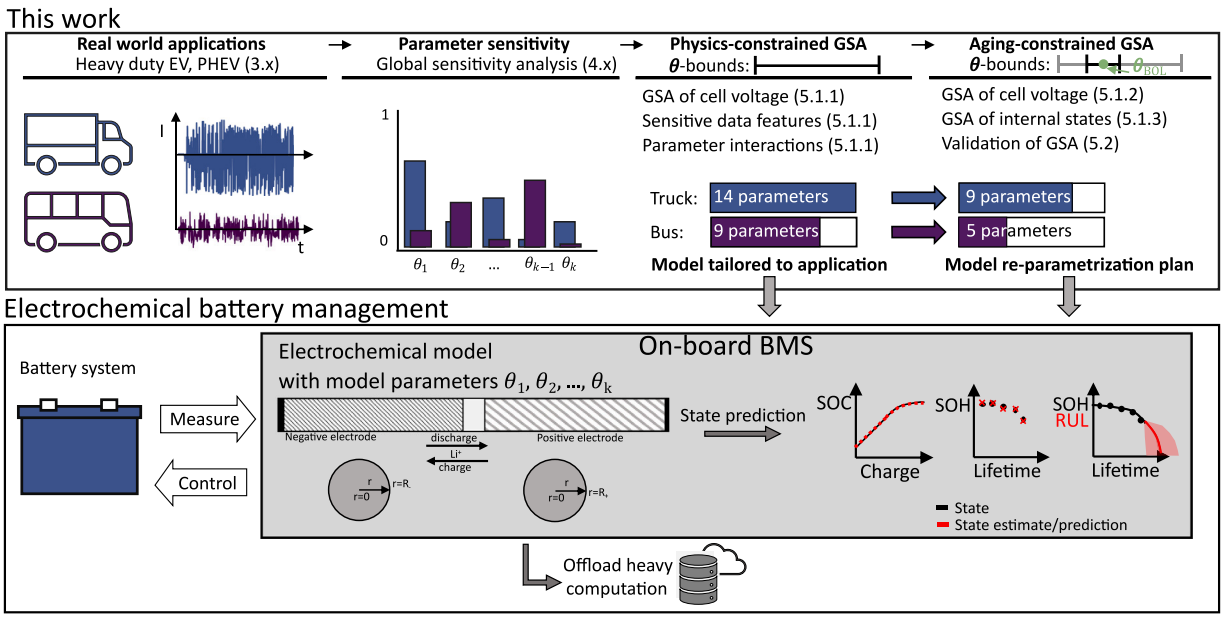

Fig. 1. This work's contribution in the context of electrochemical battery management. Electrochemical model parameters must be updated to maintain accurate state estimates as the battery ages. We performed global sensitivity analysis (GSA) to investigate how different heavy-duty driving cases affect parameter sensitivity. First, we assumed that the parameters could take on any physically motivated values (physics-constrained parameter bounds). Second, we performed a case study based on assumed beginning-of-life (BOL) parameter values as well as aging-related changes (aging-constrained parameter bounds). The sections in which the respective methods and results are discussed are noted in parenthesis.

that are invasive and dependent on special laboratory equipment and experimental procedures [18].

Dai et al. [4] suggested SOH dependent lookup tables to re-parametrize equivalent circuit models in BMS. This requires extensive aging studies of many different use cases in laboratory settings which, in addition to demanding significant resources, does not match current EV development timelines. In electrochemical models certain well-understood aging processes can be described phenomenologically [19,20] but this requires even more parameters and still cannot fully capture the complexity of battery degradation [2,21]. Bi et al. [8] used aging models to track four changing model parameters online but corrected the model predictions based on measurements of cell voltage. A third option for re-parametrization is to identify model parameters from input–output data measured on-board. This has been successfully implemented for equivalent circuit models, both with recursive methods [22] and curve fitting of collected data-sets [23]. As model complexity grows, separation of the voltage measurement into individual mechanistic contributions becomes increasingly difficult as many mechanisms cause similar model responses. This makes parametrization challenging, especially in online settings where input data is limited by vehicle usage and measurement quality limited by sensor accuracy.

Sensitivity and identifiability of parameters in electrochemical battery models have been extensively studied [18]. However, few works have investigated which model parameters are most important to describe batteries used in EVs or which parameters are identifiable from on-board vehicle data. Li et al. [24] studied the parameter sensitivity to cell voltage as well as other internal battery states to evaluate if parameters important for internal state prediction are also identifiable. Gao et al. [25] used a SA to study the importance of model parameters for cell voltage at different temperature and SOH to determine which parameters can be identified at different conditions. Bi et al. [8] performed SA to cell voltage to determine which parameters could be updated based on voltage measurements. Previous authors studied parameter sensitivity for standard electric passenger car drive cycles. These standard cycles contain repetitive current patterns and they typically assume full depth of discharge of the batteries which is rare in real operation. The parameter sensitivity during real-use cases of heavy-duty EVs has not been studied. In this paper driving data, collected from electric and hybrid-electric heavy-duty vehicles during operation is investigated for the first time. We analyzed the sensitivity of 15 electrochemical parameters of the full order Doyle–Fuller–Newman (DFN) model [26] and propose how this can be used to simplify the re-parametrization problem in electrochemical BMS by (a) reducing model complexity (b) reducing the number of parameters to update and (c) selecting informative data-sets for re-parametrization.

Previous works have used both local [8,24] and global [25,27] SA methods to study constant current cycling [8,27] or standardized drive cycles of passenger cars [24,25]. A local SA computes the sensitivity at one point in the parameter space, by perturbing one parameter at a time from some nominal parameter values [10]. A global analysis instead varies all the parameters simultaneously within their assumed bounds and provides an average measure of a parameter's sensitivity as well as a measure of parameter interactions. Global methods are computationally demanding but provide more information about a parameter's impact on model output than local SA in the presence of parameter uncertainty, model non-linearity and parameter interactions [28,29]. The DFN model is known to be non-linear [30] and to contain interactions [31]. In addition, many of its parameters can take on values in large spans [32] and change significantly [9] during life. In our study, we take this parameter uncertainty into account and therefore choose a global sensitivity analysis (GSA) for our analysis. To this end, the main contributions of this work are:

- GSA of DFN model parameters to cell voltage, using a polynomial chaos expansion (PCE) approximation of Sobol's method. The results indicate which parameters are identifiable from driving data, which parameters must be grouped due to interaction, and which parameters are essential for model performance.
- GSA with respect to current from three different types of heavy-duty vehicles and a correlation analysis between parameter sensitivity and features in driving data. This highlights how specific vehicle usage influences parameter importance.

Table 1
Governing equations for the DFN model. Variables and parameters are explained in Table 2.

Equations	Boundary condition	Eq. no.
Li$^+$ transport in electrolyte phase		
$\frac{\partial \varepsilon_{e,\pm} c_e}{\partial t} + \nabla \cdot \left(-D_{e,\pm}^{eff} \nabla c_e\right) = \left(\frac{1-t_+^0}{F}\right) i_{tot}$	$\frac{\partial c_e}{\partial x}\|_{x=0,L} = 0$	(1),(2)
$D_{e,\pm}^{eff}(c_e) = D_e(c_e)\frac{\varepsilon_{e,\pm}}{\tau_{e,\pm}}$		(3)
$i_{tot} = i_{loc,\pm} a_\pm$		(4)
$a_\pm = \frac{3\varepsilon_{a,\pm}}{R_\pm}$		(5)
Charge conservation		
Electrode phase:		
$\nabla \cdot \left(-\sigma_{a,\pm}^{eff} \nabla \Phi_\pm\right) = -i_{tot}$	$\Phi_-\|_{x=0} = 0$ $\sigma_-^{eff} \frac{\partial \Phi_-}{\partial x}\|_{x=L_-} = 0$ $\sigma_+^{eff} \frac{\partial \Phi_+}{\partial x}\|_{x=L_-+L_s} = 0$ $\sigma_+^{eff} \frac{\partial \Phi_+}{\partial x}\|_{x=L} = -\frac{I_{cell}}{A_{cell}}$	(6),(7)
$\sigma_{a,\pm}^{eff} = \sigma_{a,\pm}\frac{\varepsilon_{a,\pm}}{\tau_{a,\pm}}$		(8)
Electrolyte phase:		
$\nabla \cdot \left(-\kappa_{\pm^{eff}} \nabla \Phi_e\right) + \nabla \cdot \left(\kappa_{D,\pm}^{eff} \nabla \ln c_e\right) = i_{tot}$	$\frac{\partial \Phi_e}{\partial x}\|_{x=0,L} = 0$ $\frac{\partial c_e}{\partial x}\|_{x=0,L} = 0$	(9),(10)
$\kappa_\pm^{eff}(c_e) = \kappa_e(c_e)\frac{\varepsilon_{e,\pm}}{\tau_{e,\pm}}$		(11)
$\kappa_{D,\pm}^{eff} = \frac{2RT\kappa_\pm^{eff}}{F}\left(1 + \frac{\partial \ln f_\pm}{\partial \ln c_e}\right)(1 - t_+^0)$		(12)
Charge transfer kinetics		
$i_{loc,\pm} = i_{0,\pm}\left[exp\left(\frac{\alpha_{a,\pm} F}{RT}\eta_\pm\right) - exp\left(-\frac{\alpha_{c,\pm} F}{RT}\eta_\pm\right)\right]$		(13)
$i_{0,\pm} = F k_\pm (c_{max,\pm} - c_{surf,\pm})^{\alpha_{a,\pm}} (c_{surf,\pm})^{\alpha_{c,\pm}} \left(\frac{c_e}{c_{e,0}}\right)^{\alpha_{a,\pm}}$		(14)
$\eta_\pm = \Phi_\pm - \Phi_e - U_\pm - i_{loc,\pm} R_{film}$		(15)
$R_{film,-} = \frac{t_{SEI}}{\kappa_{SEI}}$, $R_{film,+} = 0$		
Lithium transport in particle domain		
$\frac{\partial c_\pm}{\partial t} = \frac{1}{r_\pm^2}\frac{\partial}{\partial r}\left(D_\pm r_\pm^2 \frac{\partial c_\pm}{\partial r}\right)$	$\frac{\partial c_\pm}{\partial r}\|_{r=0} = 0$ $D_\pm \frac{\partial c_\pm}{\partial r}\|_{r=R_\pm} = -\frac{i_{loc,\pm}}{F}$	(16), (17)
$t_\pm = \frac{r_\pm^2}{D_\pm}$		(18)
Porous media properties		
$\tau_{a,\pm} = \varepsilon_{a,\pm}^{1-Br_{a,\pm}}$		(19)
$\tau_{e,\pm} = \varepsilon_{e,\pm}^{1-Br_{e,\pm}}$		(20)
$\varepsilon_{a,\pm} + \varepsilon_{e,\pm} + \varepsilon_{ia,\pm} = 1$		(21)
Cell voltage		
$U_{cell} = \phi_+\|_{x=L} - \phi_-\|_{x=0} - I_{cell} R_{cc} A_0$		(22)
Cell balancing		
$q_\pm = \varepsilon_{a,\pm} L_\pm c_{max,\pm} F A_0$		(23)
$SOL_\pm = \frac{c_\pm}{c_{max,\pm}}$		(24)
$Li_{cyc} = \frac{q_{Li}}{q_+}$		(25)
$SOL_+ = Li_{cyc} - SOL_-\frac{q_-}{q_+}$		(26)
$OCV = U_+(SOL_+) - U_-(SOL_-)$		(27)

- GSA with respect to internal battery states such as the lithium plating potential. This shows the impact of parameter uncertainty on accurate electrochemical control.
- Parameter estimation on a synthetic voltage measurement based on real vehicle driving validates the conclusions from the GSA and highlights the importance of quantifying interaction for unique parametrization.

The DFN model is described in Section 2.1 along with a motivation of the studied parameters and their assumed bounds. The internal states that we study are presented in 2.3. In Section 3 the characteristics of the driving data-sets are described. Section 4 contains a thorough description of the used SA method. All results are presented in Section 5 and finally, Section 6 contains our main conclusions. Fig. 1 shows the contributions of this paper in the context of model-based electrochemical battery management.

2. Electrochemical battery model

2.1. Model formulation

We used the commonly applied DFN model [26]. This pseudo-two-dimensional model considers a porous electrode-separator-electrode domain and a secondary pseudo-particle-domain. The primary domain encompasses an active material solid phase, an inactive material solid phase, and an electrolyte phase. Transport of ions through the electrolyte is considered by diffusion and migration (Eq. 1). The potential distribution in the electrolyte (Eq. 9) and electrode (Eq. 6) phases is evaluated with Ohm's law. Transport properties in the electrolyte and electrode are adjusted with a tortuosity factor to take the porous structure into account (Eqs. 3, 8, 11). Mass transport in the pseudo-particle-domain is idealized as solid diffusion in spherical particles and

described with Fick's law (Eq. 16). The two domains are coupled by a reaction on the particles' surfaces which is described with Butler–Volmer kinetics (Eq. 13). We considered concentration dependence in the exchange current density (Eq. 14). The inactive material comprises conductive additives, binder, and inactive side-reaction products. Model equations and boundary conditions are stated in Table 1. The coupled set of partial differential algebraic equations was solved numerically using the PyBaMM python package [33]. The initial cell voltage was fixed according to the performed experiment. This matches the real-world case where batteries are generally controlled by voltage.

2.2. Model parameters

Model parameters for the employed DFN model are given in Table 2. Many parameters have significant dependencies on SOC, temperature, SOH or are distributed within the electrode domain [18]. These dependencies cannot be determined trivially and are therefore often significantly simplified or not considered. In this paper, we assumed isothermal operating-conditions and no aging occurring during a single experiment. Furthermore, diffusion coefficients and rate constants were assumed to be independent of SOC in both electrodes. The parameters included in the sensitivity analyses are those assumed to change with aging, i.e., neither material properties nor geometrical properties that are approximately constant throughout the lifetime were considered. A commercially available automotive cell was used as basis for the parametrization. The open circuit potential (OCP) curves were obtained from measurements. Additional rudimentary characterization was used to determine geometric properties of the cell, i.e., the separator and electrode thicknesses and cross sectional areas. Electrolyte properties were considered constant and changing porous structure was instead included by sampling the Bruggeman coefficients in both electrodes and the separator. The particle radius is relevant both for the diffusion length (Eq. 16) in the pseudo-domain and for the active material surface area (Eq. 5). To ensure sampled parameters are structurally identifiable, we fixed the radii and investigated active material diffusion time constants (Eq. 18) in both positive and negative electrode. Electrode kinetics were considered by sampling rate constants in both electrodes. Aging related changes in electrode balancing by loss of lithium inventory or loss of active material were included by sampling volume fractions in both electrodes and a cyclable lithium parameter (Eq. 25). Power fade was investigated by sampling e.g., the thickness of the solid-electrolyte-interphase which adds a distributed resistance on the negative particle surface. On the positive electrode, a contact resistance between active material and current collector was included.

Note that for some parameters, their importance lies in contributions to different effects. The electrolyte volume fractions are for instance present in four distinct processes. Firstly, they directly relate to the electrolyte mass transport by diffusion and migration (Eq. 1) and the electrolyte tortuosity (Eq. 20). Through their impact on the active material volume fraction they are also responsible for the interfacial surface area (Eq. 5) and the electrode capacities (Eq. 23). If all four mechanisms are important, a unique parametrization exists.

We summarize the parameters included in the GSA in Table 3. The result of a GSA is highly dependent on the ranges that each parameter is assumed to vary within. First, we studied high parameter uncertainty to minimize the prior assumptions about any of the parameters. In this case, we delimited possible parameter values by ranges found in literature or physics-based limitations. We denote this case the physics-constrained GSA (PC-GSA). The second case reflects a situation in which the BOL parametrization of a cell is known. The parameter ranges represent the change in each parameter that can occur during the life of the cell. This required an assumption about the BOL values of some of the parameters, whereupon we refer to this study as aging-constrained GSA (AC-GSA). Note that for parameters where sampled ranges span more than one order of magnitude, the exponent of the parameter was used instead. For the sake of readability, these parameters are referred to by their original name in the remainder of this text.

2.3. Internal states

The importance of the parameters in Section 2.2 was evaluated by means of their sensitivity to the cell voltage as well as various battery states. We selected four states for the SA: the interfacial potential, the electrolyte concentration, the average particle concentration as well as the particle surface concentration. These are states that govern degradation and performance of the cell, via their effect on e.g. reaction rates [42,43], electrode utilization [44], volume expansion [45], material stability [46] as well as conductive and diffusive properties [47]. The analyzed states are summarized in Table 4, where the interfacial potential is defined as $\phi_{i,\pm} = U_{\pm} + \eta_{\pm}$ (from Eq. (15)). We analyzed all states in two spatial locations in each electrode; at the electrode-separator interface and at the electrode-current collector (CC) interface. These locations correspond to the states' extreme points and are thus the most important to monitor.

3. Input data

The input signals were collected from measurements of the battery current on board electric heavy-duty vehicles. They thus contain dynamics produced by real vehicles in operation. It is outside the scope of this study to explore parameter sensitivities to a broad variety of EV load cycles or to investigate characteristics of typical EV operation. Instead, three current time-series were selected from three distinct vehicles that all use the same battery cell. In addition, two charging events were considered: one fast and one slow. The start OCV we used for each set is listed in Table 5. The investigated data-sets are shown in Fig. 2.

The current was measured at 100 Hz on-board the vehicles. Due to computational limitations, we could not perform the GSA on the data-sets using 100 Hz. We therefore down-sampled the current and investigated the impact of input signal frequency by performing sensitivity analysis on three input signal cases; 0.1 Hz, 1 Hz and 10 Hz sampling. The result showed only marginal differences in variance measures, and the subsequent studies were performed on the 1 Hz input signal, which facilitated the SA and the data handling.

Because the current signal is an on-board measurement, it contains measurement noise. A majorization-minimization algorithm from [48] was employed for noise removal before down-sampling.

3.1. Battery electric vehicle (BEV) distribution truck

The first data-set was collected from a BEV truck that was driven like a distribution truck. The set, shown in Fig. 2(a), includes shorter segments of highway driving as well as operation in an urban area with slow speed and idling. Charging power was supplied by regenerative breaking that converts kinetic energy from the wheels to electric energy. In addition, the data-set contains a fast charging event.

3.2. BEV city bus

The second data-set, Fig. 2(b), originates from a BEV bus that was driven on a city bus route. This type of operation is characterized by low and medium speed as well as frequent acceleration and de-acceleration. The vehicle was equipped with more battery cells in parallel than the BEV truck and thus the current seen by each cell was lower. On each end station of the route, there was a fast charger where the bus could be charged. These short charges did not bring the battery back to 100% SOC but were enough to keep the vehicle operational and only reach low SOC after many hours. We selected one of the driving segments for our study.

Table 2
DFN Model parameters and their nominal values. Parameters included in the GSA sampling are denoted with s. Reference is given where applicable, measured parameters are denoted with m and assumed parameters with a.

Parameter	Description	Value	Source
	Dependent variables		
$\Phi_{\pm}$	Potential in the solid phase		
Φ_e	Potential in the electrolyte phase		
$c_{\pm}$	Concentration in the active material		
c_e	Concentration in the electrolyte		
	Particle Domain	+, -	
$r_{\pm}$	Particle radius		m, m
$t_{\pm}$	Solid diffusion time constant	s, s	
	Electrode Domain		
	Electrolyte properties		
D_e	Electrolyte diffusion coefficient	$f(c_e, T)$	[34]
κ_e	Ionic conductivity	$f(c_e, T)$	[34]
t_+^0	Cationic transference number	$f(c_e, T)$	[34]
$1 + \frac{\partial f_{\pm}}{\partial \ln c_e}$	Electrolyte activity coefficient	$f(c_e, T)$	[34]
$\tau_{e,\pm}$	Electrolyte tortuosity	Eq. (20)	
$Br_{e,\pm}$	Electrolyte Bruggeman coefficient	s	
$\varepsilon_{e,\pm}$	Electrolyte volume fraction	s	
	Active material properties		
$\sigma_{a,\pm}$	Electronic conductivity	100 S/m	[35]
$\tau_{a,\pm}$	Electrode tortuosity	Eq. (19)	
$Br_{a,\pm}$	Electrode Bruggeman coefficient	1.5	a
$k_{\pm}$	Reaction rate constant	s	
$\alpha_{a,\pm}, \alpha_{c,\pm}$	Anodic/cathodic charge transfer coefficient	0.5	[35]
$U_{\pm}$	Open circuit potential	$f(c_{\pm})$	m
$\varepsilon_{a,\pm}$	Active material volume fraction	Eq. (21)	
$L_{\pm}$	Electrode thickness		m
$a_{\pm}$	Volume specific electrode area	Eq. (5)	
$c_{max,\pm}$	Maximum lithium concentration in active material	50.3 kmol/m^3, 28.6 kmol/m^3	a
$c_{init,\pm}$	Initial lithium concentration in active material	Eqs. (23)–(27)	
t_{SEI}	SEI layer thickness	s	
κ_{SEI}	SEI layer conductivity	5×10^{-6} S/m	[36]
	Inactive material properties		
$\varepsilon_{ia,\pm}$	Inactive material volume fraction	s	
	Separator Domain		
ε_s	Separator porosity	0.4	[37]
τ_s	Separator tortuosity	Eq. (20)	
Br_s	Separator Bruggeman coefficient	s	
L_s	Separator thickness	20 μm	a
	Other cell properties and constants		
R_{cc}	Current collector contact resistance positive electrode	s	
A_0	Total cell surface area		m
F	Faraday constant	96845 C/mol	

Table 3
Model parameters included in the SA where *a* denotes assumed values and * denotes ranges adjusted from the given reference. PC-GSA bounds correspond to the case where very little is known about a battery and AC-GSA bounds incorporate parameter changes possible during aging. We sampled the exponents of parameters where ranges differ more than one order of magnitude. They are denoted as p.

θ_i	Meaning	Range PC-GSA	Range AC-GSA	Ref
$p_{t,+}$	Exponent of positive electrode diffusion time constant	[0 ... 3.5]	[0.59 ... 1.18]	[31], [38]
$p_{t,-}$	Exponent of negative electrode diffusion time constant	[2.8 ... 3.9]	[2.86 ... 3.41]	[31], [38]
$\varepsilon_{e,+}$	Electrolyte volume fraction in positive electrode	[0.25 ... 0.4]	[0.25 ... 0.35]	[32]*, a
$\varepsilon_{e,-}$	Electrolyte volume fraction in negative electrode	[0.2 ... 0.4]	[0.23 ... 0.33]	[32]*, a
$\varepsilon_{ia,+}$	Positive electrode inactive material volume fraction	[0.1 ... 0.2]	[0.1 ... 0.2]	a, a
$\varepsilon_{ia,-}$	Negative electrode inactive material volume fraction	[0.05 ... 0.15]	[0.05 ... 0.15]	a, a
$Br_{e,+}$	Positive electrode Bruggeman coefficient	[1.5 ... 3]	[2.1 ... 2.6]	[32]*, a
$Br_{e,-}$	Negative electrode Bruggeman coefficient	[1.5 ... 3]	[2.1 ... 2.6]	[32]*, a
$Br_{e,s}$	Separator Bruggeman coefficient	[1.5 ... 3]	[2.1 ... 2.6]	[32]*, a
$p_{k,+}$	Exponent of positive electrode kinetic rate constant	[-7 ... -4]	[-6 ... -5]	[32]*
$p_{k,-}$	Exponent of negative electrode kinetic rate constant	[-7 ... -4]	[-5 ... -4]	[32]*
$p_{t,SEI}$	SEI thickness exponent	[-8.3 ... −6.3]	[-8.3 ... −6.3]	[36,39,40]
$p_{R,cc}$	Positive electrode contact resistance exponent	[-5 ... -3]	[-5 ... -3]	[41]
Li_{cyc}	Normalized cyclable lithium	[0.95 ... 1]	[0.95 ... 1]	a

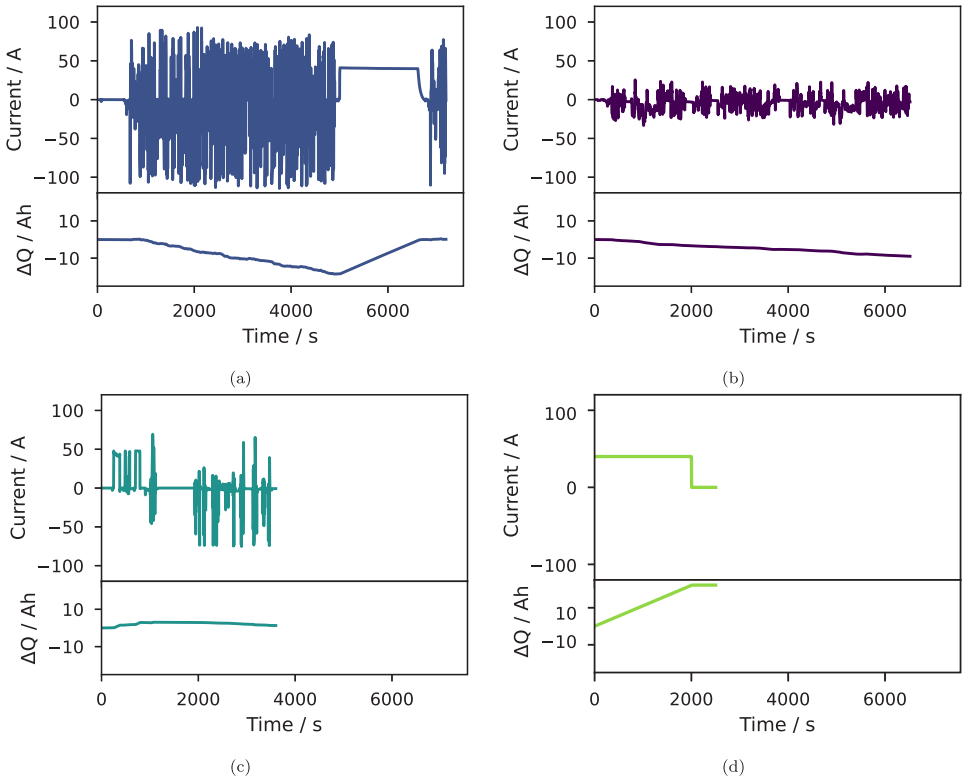

Fig. 2. Measured current signals from a BEV distribution truck (a), a BEV city bus (b), a PHEV distribution truck (c) and fast charging (d). Slow charging is not displayed, its current magnitude is 10% of the fast charge and the cycled capacity is equal.

Table 4
Internal states included in SA.

State	Description	Unit
$c_{e,-}\|_s$	Negative electrolyte concentration at separator	mol/m^3
$c_{e,-}\|_{CC}$	Negative electrolyte concentration at CC	mol/m^3
$c_{e,+}\|_s$	Positive electrolyte concentration at separator	mol/m^3
$c_{e,+}\|_{CC}$	Positive electrolyte concentration at CC	mol/m^3
$c_{surf,-}\|_s$	Negative particle surface concentration at separator	mol/m^3
$c_{surf,-}\|_{CC}$	Negative particle surface concentration at CC	mol/m^3
$c_{surf,+}\|_s$	Positive particle surface concentration at separator	mol/m^3
$c_{surf,+}\|_{CC}$	Positive particle surface concentration at CC	mol/m^3
$c_{avg,-}\|_s$	Negative particle average concentration at separator	mol/m^3
$c_{avg,-}\|_{CC}$	Negative particle average concentration at CC	mol/m^3
$c_{avg,-}\|_s$	Positive particle average concentration at separator	mol/m^3
$c_{avg,-}\|_{CC}$	Positive particle average concentration at CC	mol/m^3
$\phi_{i,-}\|_s$	Negative interfacial potential at separator	V
$\phi_{i,-}\|_{CC}$	Negative interfacial potential at CC	V
$\phi_{i,+}\|_s$	Positive interfacial potential at separator	V
$\phi_{i,+}\|_{CC}$	Positive interfacial potential at CC	V

Table 5
Start OCV for the SA of the different data-sets.

Data-set	OCV
BEV truck	3.821 V
BEV bus	4.000 V
PHEV truck	3.650 V
Fast charge	3.500 V
Slow charge	3.500 V

3.3. Plugin hybrid electric vehicle (PHEV) truck

The third data-set comes from a PHEV truck (Fig. 2(c)). The hybrid vehicle can be driven both as a BEV as well as in hybrid mode, which means that the battery and the internal combustion engine split the vehicle's power demand. Since the data contains long periods of zero current, the current signal in Fig. 2(c) was constructed by concatenating several different segments.

3.4. Charging

In addition to the sets collected from real vehicles in operation, a fast charge and a slow charge was also investigated. During the fast charge, a constant current of 40 A was applied during 2000 s. The slow charge consisted of constant 4 A during 20 000 s. The fast charge ended with a 500 s rest period whereas the slow charge was followed by 100 s of rest.

4. Sensitivity analysis

4.1. Variance based global sensitivity analysis

For the GSA we used Sobol's method, which is a technique that decomposes the output variance into contributions from the different parameters and parameter interactions [49]. It studies how a given parameter uncertainty produces uncertainty in the output. The basis for the method is to assume that the output $y(t,\theta)$ can be expanded as

$$y(t,\theta) = y_0(t) + \sum_{j=1}^{N_\theta} y_j(t,\theta_j) + \sum_{j=1}^{N_\theta}\sum_{k>j}^{N_\theta} y_{k,j}(t,\theta_k,\theta_j) + \cdots + y_{1,2\ldots N_\theta} \quad , \quad (28)$$

where $y_j(t,\theta_j)$ is the individual contribution from parameter θ_j, $y_{k,j}(t,\theta_k,\theta_j)$ is the contribution from interaction between parameters θ_k and θ_j and so forth [50]. The term $y_0(t)$ is the expected value of $y(t,\theta)$ and independent of the parameters $\boldsymbol{\theta}$. This entails that the expectations of all the other terms in (28) must be zero in order for the decomposition to hold. Assuming that the parameters are uniformly distributed in their given ranges and that the output $y(t,\theta)$ is

continuously differentiable and square integrable, the variance of $y(t,\boldsymbol{\theta})$ can be computed as [50]

$$V(t) = \sum_{j=1}^{N_\theta} V_j(t) + \sum_{j=1}^{N_\theta}\sum_{k>j}^{N_\theta} V_{k,j}(t) + \cdots + V_{1,2,\ldots,N_\theta}(t) \quad . \tag{29}$$

$V_j(t)$ is the first-order variance contribution corresponding to parameter θ_j while $V_{k,j}(t)$ is the second order variance contribution from interaction between θ_k and θ_j [49]. It is also common to evaluate the total effect of θ_j, defined by [51]

$$V_{Tj}(t) = V_j(t) + \sum_{k\neq j} V_{k,j}(t) + \cdots V_{1,2,\ldots,N_\theta}(t) \quad . \tag{30}$$

4.2. Polynomial chaos expansion

Commonly, Monte Carlo methods are employed to calculate the Sobol indices. Computation of first-order and total effects requires about $N(N_\theta+2)$ simulations, where N is in the range of 500-1000 [52]. A simulation with the battery model is computationally costly, which limits the feasibility of extensive global sensitivity analyses. To facilitate investigation of several data-sets, sampling frequencies and constant parameter sets, we used polynomial chaos expansion (PCE) [53] to reduce the number of required simulations.

The basis for PCE is to approximate the model $y(\boldsymbol{\theta})$ with a linear combination of orthogonal polynomials $\Psi_m(\boldsymbol{\theta})$ such that

$$y(\boldsymbol{\theta}) \approx \sum_{m=0}^{P} \alpha_m \Psi_m(\boldsymbol{\theta}) \quad . \tag{31}$$

Here, α_m are polynomial coefficients. The number of required polynomials P+1 is computed from

$$P = \frac{(N_\theta + p)!}{N_\theta! p!} - 1 \quad , \tag{32}$$

where p is the order of the PCE [53]. The polynomials $\Psi_m(\boldsymbol{\theta})$ are in their turn obtained from the product of one-dimensional orthogonal polynomials $\psi_j(\theta_j)$:

$$\Psi_m(\boldsymbol{\theta}) = \psi_1^{m_1}(\theta_1)\psi_2^{m_2}(\theta_2)\ldots\psi_{N_\theta}^{m_{N_\theta}}(\theta_{N_\theta}) \quad . \tag{33}$$

These are chosen based on the distribution of the parameters [53]. The superscripts m_j signifies the order of the polynomials. For $m = 0$, all univariate polynomials are of order zero and $\Psi_0(\boldsymbol{\theta}) = 1$. The expectation of $y(\boldsymbol{\theta})$ can be computed as

$$\begin{aligned} E[y(\boldsymbol{\theta})] &= \int y(\boldsymbol{\theta}) p(\boldsymbol{\theta}) d\boldsymbol{\theta} = \int \Big(\sum_{m=0}^{P} \alpha_m \Psi_m(\boldsymbol{\theta})\Big) p(\boldsymbol{\theta}) d\boldsymbol{\theta} \\ &= \sum_{m=0}^{P} \alpha_m \int \Psi_0(\boldsymbol{\theta}) \Psi_m(\boldsymbol{\theta}) p(\boldsymbol{\theta}) d\boldsymbol{\theta} \end{aligned} \tag{34}$$

where $p(\cdot)$ is the probability density function (PDF). From the definition of orthogonality,

$$\int \Psi_q(\boldsymbol{\theta}) \Psi_m(\boldsymbol{\theta}) p(\boldsymbol{\theta}) d\boldsymbol{\theta} = \begin{cases} 0 & m \neq q \\ 1 & m = q \end{cases} \tag{35}$$

which gives

$$E[y(\boldsymbol{\theta})] = \alpha_0 \quad . \tag{36}$$

The variance in Eq. (29) can similarly be computed from

$$V[y(\boldsymbol{\theta})] = \int \Big(\sum_{m=0}^{P} \alpha_m \Psi_m(\boldsymbol{\theta}) - \alpha_0\Big)^2 p(\boldsymbol{\theta}) d\boldsymbol{\theta} = \sum_{m=1}^{P} \alpha_m^2. \tag{37}$$

The last equality is a result of Eq. (35), that makes all cross-terms in the square disappear. The components of the variance in Eq. (29) are

$$V_j = \sum_{m\in M_j} \alpha_m^2 \tag{38}$$

$$V_{k,j} = \sum_{m\in M_{k,j}} \alpha_m^2 \tag{39}$$

$$V_{T_j} = \sum_{m\in M_{Tj}} \alpha_m^2 \quad , \tag{40}$$

where M_j contains all products where only $m_j \neq 0$, $M_{k,j}$ the ones where only m_k and $m_j \neq 0$ and M_{Tj} all the ones where $m_j \neq 0$ [27].

The coefficients α_m were fitted to simulated model output for different parameter values using the python implementation of PCE in [54]. We included first- and second-order interactions. A total of 2480 different samples of the parameter vector were used to produce corresponding model output sequences. To obtain parameter sets with low discrepancy, we used latin-hypercube-sampling (LHS) [55]. Since we assigned wide parameter ranges, some parameter combinations were not feasible and thus caused model simulations to crash. We excluded those parameter samples from the computation of the PCE coefficients. The BEV truck data-set had the highest number of unfeasible parameter samples and resulted in 20 unusable parameter sets (0.8%) for the PC-GSA bounds and 0 unusable samples for the AC-GSA bounds. The common denominator for the unfeasible parameter sets was high positive porosity, high positive inactive material volume fraction and high negative diffusion time constant. This causes low positive hosting capacity and thus a big voltage drop at the very end of the BEV truck driving event. It is therefore possible that the variance contribution of the positive porosity, inactive material volume fraction and negative diffusion time constant would be higher at the end of the discharge, if it was possible to simulate those samples. Refer to the supplementary material (Fig. A.4) for a figure of the unfeasible parameter samples.

5. Results and discussion

5.1. Sensitivity analysis

5.1.1. Physics-constrained bounds

Fig. 3(a) displays the first-order voltage variance contribution from the parameters on the BEV distribution truck data-set. The result was obtained using the PC-GSA parameter bounds, with few prior assumptions on the parameters. The y-axes are logarithmic to highlight the large spread in variance and individual parameters' contributions. We assumed on-board voltage measurements to include Gaussian noise with a $\sigma = 5$ mV standard deviation. Parameters with variance contribution above noise level were considered sensitive. A gray dashed line was therefore included at σ^2 to highlight the sensitivity threshold.

When comparing the parameter contributions to cell voltage variance with the drive cycle in Fig. 2(a), it can immediately be observed that driving (<4200 s) or charging (4200–6000 s) behavior has significant impact on which battery-internal processes are important. All parameters exceeded the noise level at some point during the BEV truck experiment. However, the contributions varied several orders of magnitude, with ohmic, kinetic and capacity/balancing parameters having larger impact than Bruggeman coefficients and diffusion time constants.

To study which property of the driving data makes parameters sensitive, we defined several features and studied their correlation with the observable variance. Fig. 3(b) shows the linear correlation between the first-order variance and three relevant features of the input data.

Firstly, we identified the passed charge to correlate with capacity related and SOC dependent parameters. Secondly, the current magnitude correlated strongly with ohmic and kinetic parameters and influences the current distribution in the electrolyte. Lastly, a polarization time was included to capture parameters that increase in importance when the electrolyte or particle concentration gradients are large. These correlations are directly related to the model, but are only general within the investigated SOC, current and dynamics range. It is for instance likely that the negative electrode diffusion time constant sensitivity

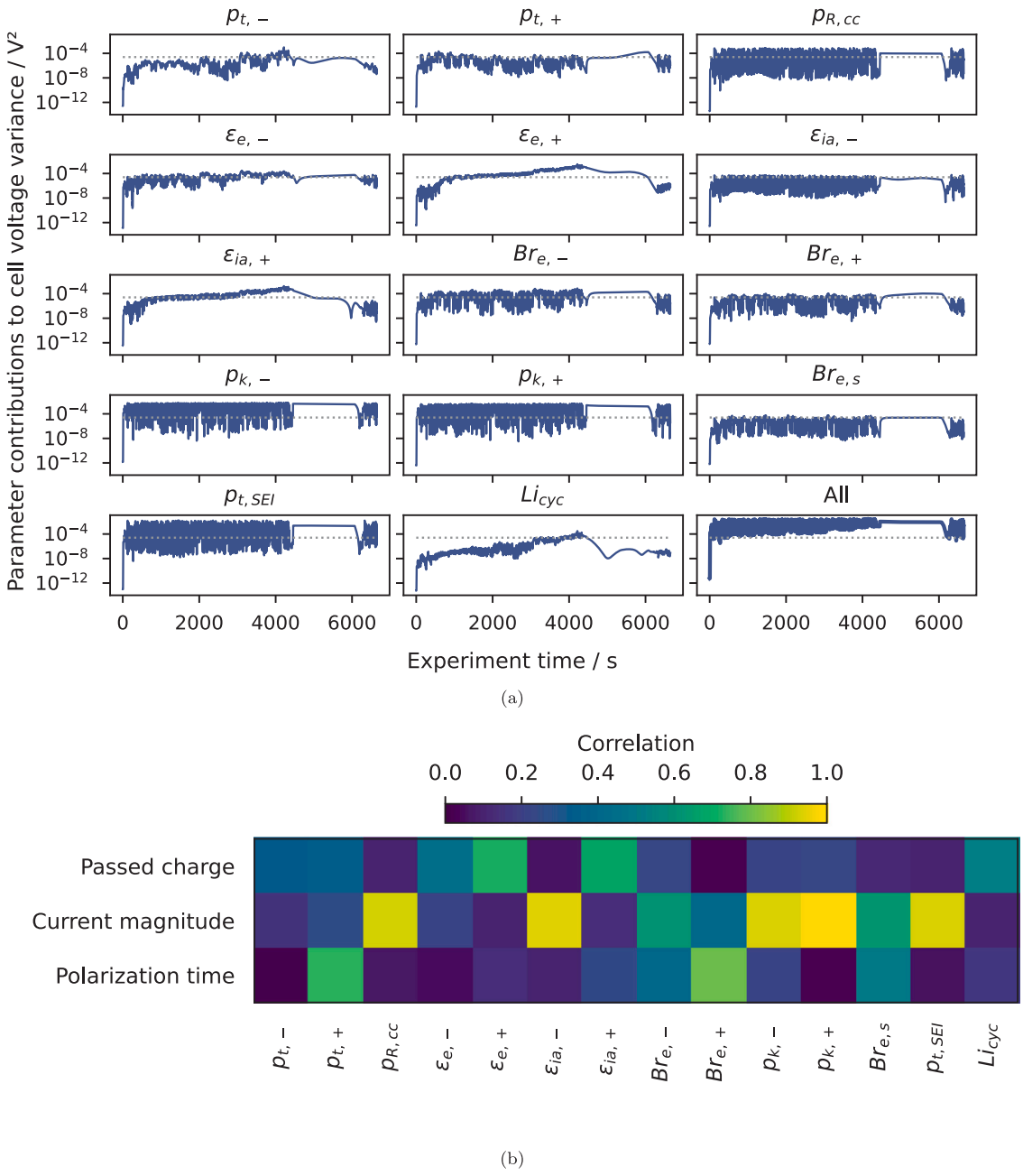

(a)

(b)

Fig. 3. (a) shows the first order contributions to cell voltage variance for the BEV distribution truck data-set and the PC-GSA parameter bounds. This directly results from the computed global sensitivity indices. The scale on the y-axis is logarithmic because of the large spread in sensitivity. A gray dashed line indicates a variance of 2.5×10^{-5} V^2 which corresponds to a 5 mV standard deviation. If a parameter contributes above this line, the corresponding mechanism must be considered for an electrochemical BMS. (b) highlights the correlation between the first order variances in (a) and features in the BEV distribution truck current data. This shows how specific usage reveals different model parameters and therefore model mechanisms.

depends largely on the half-cell OCP slope and would therefore show correlation if low SOC regions were included.

These features can be used to screen large data-sets from vehicles in operation for sections of high information.

The results in Fig. 3 (b) confirm that parameter sensitivities highly depend on the current input's properties. To highlight this, we show the average (bar) and maximum (circle) total variance contributions for all studied data-sets in Fig. 4. This includes driving of the three vehicle types (BEV truck, BEV bus, and PHEV truck) as well as fast and slow charging.

The BEV truck with highest currents and a large utilized SOC window notably has the largest maximum variances for all studied parameters. Furthermore, it is the only data-set to significantly excite all 14 studied parameters. The PHEV truck data-set with high currents but small SOC window contains sufficient variance contributions by 9 parameters and falls short for those related to capacity and electrode balancing. The BEV bus data with low currents and a moderate utilized SOC window equally excites 9 parameters, exchanging sensitivity to electrode tortuosity for capacity parameters.

In the fast charge experiment 11 parameters show significant variance contribution, opposed to only 6 parameters in the slow charge experiment despite the same charge throughput. The fast charge additionally contains those parameters correlating with current magnitude (compare Fig. 3(b)).

A GSA can only with certainty determine unidentifiability due to zero sensitivity [50]. Aside from low sensitivity, identifiability issues

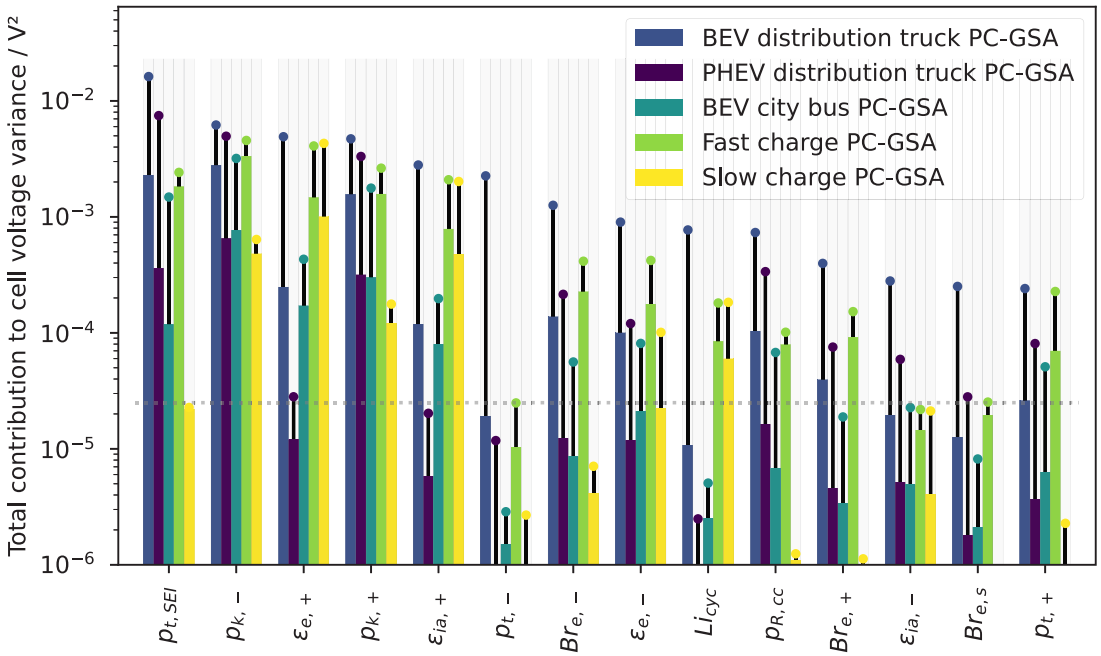

Fig. 4. Average (bar) and maximum (circle) total variance contribution to cell voltage for different studied data-sets. The result is based on the PC-GSA parameter bounds. The measurement noise level is drawn as a dotted gray line. It is evident that vehicle usage and charging strategy has significant impact on model parameter sensitivity.

can stem from parameters affecting the output indistinguishably or parameters mainly affecting the output through their interaction [56]. Low interaction is a necessary but not sufficient condition for identifiability [57]. An indication of unidentifiability is therefore the presence of significant parameter interactions. The average second-order variance contribution computed for the BEV truck data-set is displayed in Fig. 5. Interactions are mainly present for electrolyte volume fractions. This results from their relevance for electrode capacities, interfacial surface areas, and tortuosities. This effect is larger in the negative electrode, where the average interaction reaches almost 50% of the average magnitude of each first order contribution. This implies potential identifiability issues of these parameters. Interaction between electrolyte volume fractions and Bruggeman coefficients suggests that their impact on the model output to a large extent comes from the bulked electrolyte tortuosity (Eq. 20) and that it is this parameter that would be identifiable from data. Similarly, interaction between electrolyte and inactive volume fractions mean they act on the model output through the bulked active material volume fractions (Eq. 21), relevant for half-cell capacities. Interaction between SEI layer thickness and electrolyte volume fractions is caused by the latter's impact on the surface area (Eq. 5) through the active material volume fraction (Eq. 21). It would be decoupled if the tortuosity and active material volume fraction were identified instead. Quantifying interactions in this way can thus help to select uniquely identifiable parameter-sets. Only second-order interactions were included in this work due to computational limitations.

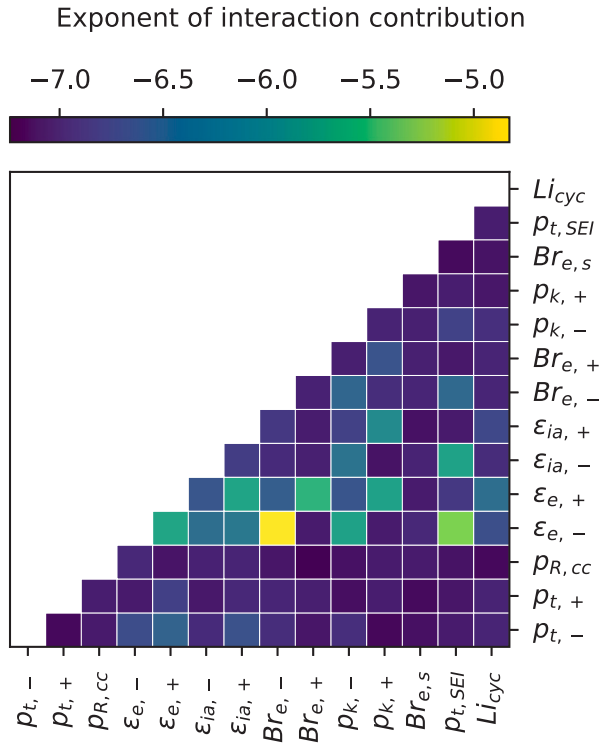

Fig. 5. Exponent of the average variance from second-order contribution to the cell voltage of BEV truck set. The PC-GSA bounds were used. A high degree of interaction (green or yellow) can cause unidentifiability, this is observed for volume fractions ε and Bruggeman coefficients. (For interpretation of the references to color in this figure legend, the reader is referred to the web version of this article.)

5.1.2. Aging-constrained bounds

The PC-GSA bounds are defined to contain any plausible parameter value and do not reflect a scenario in which BOL parameters are known. For this reason, we repeated the GSA with aging-constrained parameter intervals in the vicinity of an assumed BOL parameter set. These *aging-constrained* parameter ranges correspond to assumed changes due to battery degradation within its lifetime and are listed in Table 3. The assumed BOL parameter vector, around which the constrained samples are drawn, is taken from the PC-GSA sample that shows the lowest RMSE (5.6 mV) against the on-board voltage measurement.

The resulting change in parameter variance contribution for the BEV truck is highlighted in Fig. 6 and the equivalent results for all data-sets are given in the supplementary material (Fig. A.1). Parameters for which ranges were reduced significantly show the largest reductions in importance within the given ranges. It implies that the impact of these parameters is non-linear or dependent on other parameter values. While rate constants and porosities remain sensitive, the diffusion time

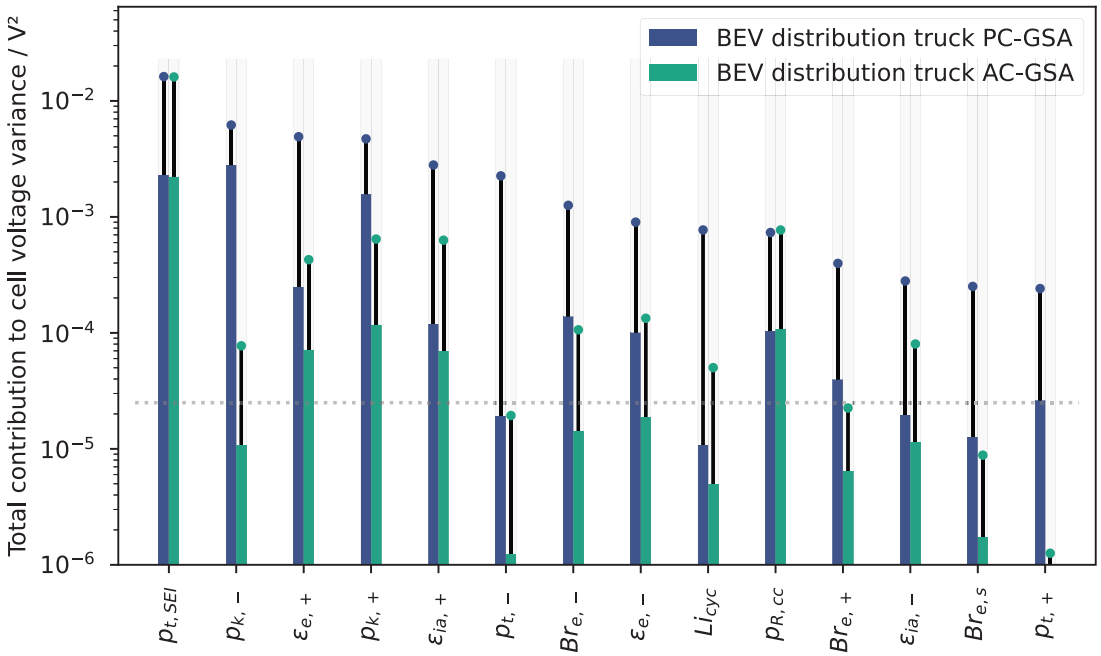

Fig. 6. Average (bar) and maximum (circle) total variance contribution for 14 studied model parameters. Constraining parameter bounds in the AC-GSA study to anticipated lifetime changes shows several effects are the same level or below measurement noise in observable data. This includes both diffusion time constants in negative and positive electrode, and Bruggeman coefficients in the positive electrode and separator. The measurement noise level is drawn as a dotted gray line.

constants in both electrodes and the Bruggeman coefficients in positive electrode and separator become insensitive. Parameter importance for all investigated driving data-sets are summarized in Fig. 7. We found significant interaction between Bruggeman coefficient and porosity as well as inactive volume fraction and porosity in both electrodes. As interaction hinders identifiability, we propose their bulked identification instead. This result is an indication for which parameters should periodically be updated but should not be generalized to any EV that might differ in BOL parameters, battery design and energy management.

Notably, no data-set significantly excites solid diffusion in either electrode. These two parameters are usually sought after and control-oriented electrochemical models such as the single particle model largely focus on solid diffusion in active material particles. Our finding indicates that if battery usage resembles the analyzed data-sets, these models focus on the incorrect processes and a better control-oriented model could instead simplify solid diffusion.

5.1.3. Global sensitivity analysis to study control on internal states

One advantage of a physics-based battery model over an empirical model is its ability to simulate internal battery states. To investigate the impact each model parameter has on the electrolyte concentration, particle surface and average lithium concentrations, and interfacial potentials, GSA was performed with these internal states as targets. For this study, the AC-GSA bounds were used to reflect parameter changes that can be expected throughout a cell's lifetime. The result summarized in Fig. 8 shows the time-averaged total effect of each parameter for the BEV truck data-set. The equivalent figures for the maximum total effect is included in the supplementary materials (Fig. A.3).

The porosities have notable impact on all internal states underlining the importance of their accuracy. The effect of varying positive porosity and positive inactive material volume fraction goes beyond the positive electrode's states as it produces variance also for the negative concentrations and potentials. The same is true in the reversed case. This can be explained by the cell balancing and fact that we initiate the simulations at the same OCV each time. It highlights how erroneous parameters can propagate and cause inaccurate state estimation in unexpected places. The diffusion time constants have little to no impact on most studied states. This aligns with previous conclusion from the cell voltage analysis that the diffusion process in particles can be simplified without loss of accuracy.

The interfacial potentials are mainly sensitive to the volume fractions, the reaction rate coefficients and the SEI thickness. Aside from the parameters that govern cell balancing, the negative particle concentrations are strongly impacted by the Bruggeman coefficient and SEI layer thickness whereas the positive concentrations are affected by the Bruggeman coefficient and reaction rate coefficients. The electrolyte concentrations are mainly impacted by electrolyte parameters ($\varepsilon_{e,\pm}$, $Br_{e,\pm}$) but also by the SEI layer thickness in the negative electrode.

Individually, the effect from most of the parameters are small. If the SEI layer thickness was the only varying parameter, it would lead to a standard deviation of the negative particle concentration corresponding to roughly 1.5%–3% of the theoretical maximum lithium concentration. This would be the order of magnitude of the SOC error, if the cell SOC was computed based on the negative average concentration (in open-loop simulation) and it shows the importance of updating the SEI thickness parameter as the cell ages. However, if more parameters were varied, the resulting electrode SOC variance becomes less straight-forward to compute, but undoubtedly larger.

Aside from the diffusion time constants, it is only the separator Bruggeman coefficient and contact resistance that do not have significant impact on any of the investigated internal states.

5.2. Validation

5.2.1. Accuracy of PCE surrogate model

First, a validation of the PCE sensitivity method was performed by generating 1000 distinct Monte-Carlo parameter samples for each data-set and comparing the PCE surrogate model to the DFN model. As the PCE constructs a polynomial representation of the investigated model state, e.g., the cell voltage, its accuracy can directly be validated by comparison with the electrochemical model's prediction of the same state. If residuals are high, the PCE representation of the target state and therefore the computed sensitivity are less accurate. The root-mean-square error (RMSE) PDFs of the resulting residuals of these 5000 simulations are given in Fig. 9 for the PC-GSA. The highest RMSE value

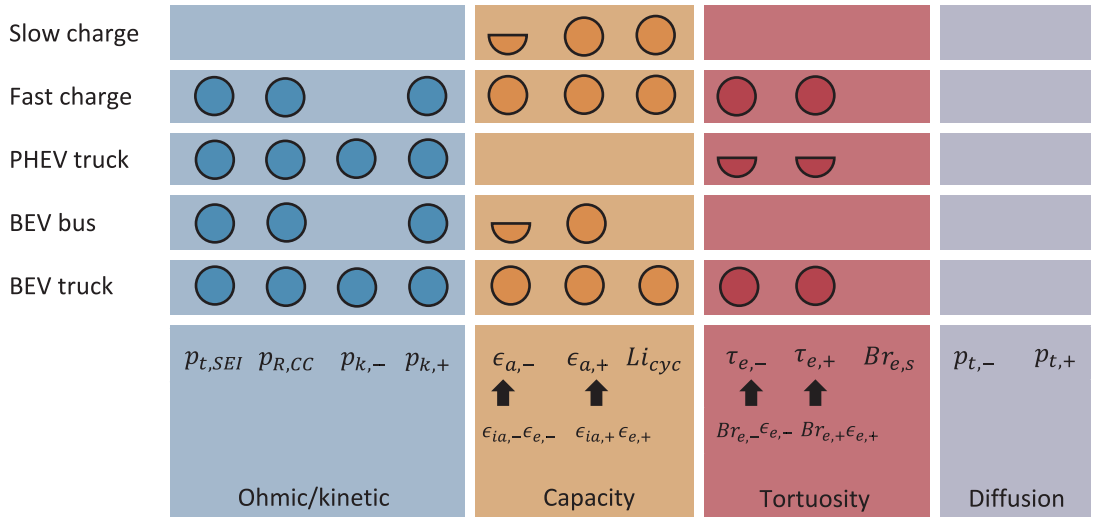

Fig. 7. Sensitive parameters depending on vehicle usage during a battery's lifetime (AC-GSA). A full circle implies high average variance contributions significantly above measurement noise and lower interaction. A semi-circle denotes bulked values where second order interaction between certain mechanisms was observed. Consider e.g. the negative electrode tortuosity $\tau_{e,-}$ where electrolyte volume fraction as well as the Bruggeman coefficient on average contribute variance on the order of the measurement noise. The second order interaction shows that for this usage, they interact significantly, supporting a bulked identification.

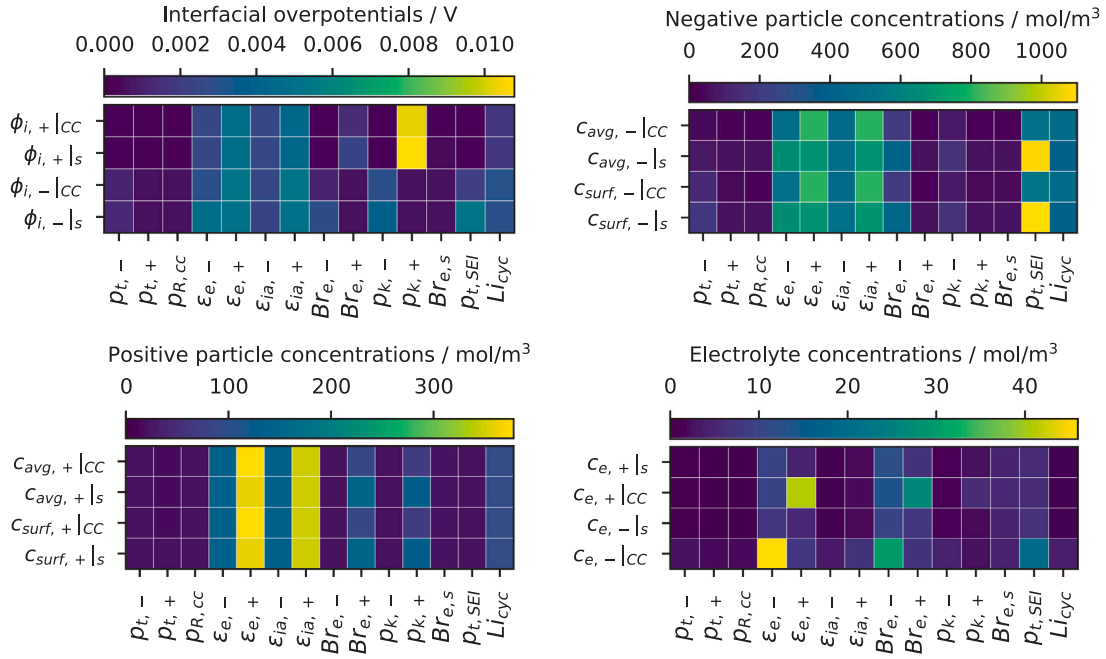

Fig. 8. Square-root of the time-averaged total variance contribution, $\sqrt{V_{Tj}}$. The AC-GSA bounds were used.

of 20.08 mV was observed for the BEV truck data-set. This specific parameter sample was in the vicinity of 20 infeasible samples that could not be computed during the PC-GSA. The same study was also performed for the AC-GSA (compare Fig. A.5), where no infeasible samples were present and BEV truck validation errors are significantly lower. The PCE approximation was therefore deemed valid except for extreme combinations of the negative diffusion time constants, positive electrode volume fractions and cyclable lithium at low SOC. This could in principle lead to an underestimation of the sensitivity of these parameters at high depth of discharge for the PC-GSA.

5.2.2. *Probing model non-linearity and parameter interactions*

A screening of cell voltage partial derivatives with respect to investigated model parameters was conducted to elucidate the parameters' non-linear impact on the cell voltage and their dependence on other parameters. This is meant to validate our choice of GSA opposed to more economical local SA approach and highlights the impact of using a global or local method on the outcome of the analysis. The normalized partial derivatives $\Delta\theta_j(\partial y(t,\boldsymbol{\theta})/\partial\theta_j)$ were computed numerically with a parameter perturbation corresponding to 0.1% of the full PC-GSA parameter span in Table 3 and the normalization factor $\Delta\theta_j$ corresponding to 10% of this span. For each parameter θ_j, five equally distributed values in the range were selected. For each of those values, 30 realizations of the other parameters were sampled with LHS. The partial derivatives were then computed for all 5×30 parameter vectors and for all 14 parameters.

The result is presented in Fig. 10. A change in the median (shown by blue lines inside the box) over the x-axis of a sub-figure indicates that the partial derivative depends on this parameter's nominal value. This is most evident in the solid diffusion time constants and reaction rate

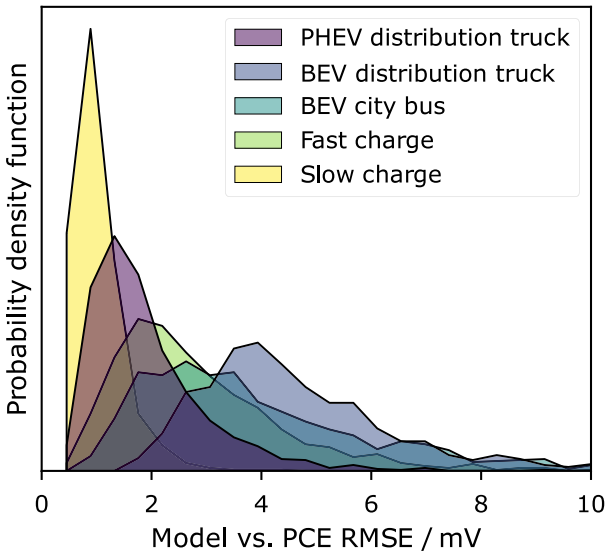

Fig. 9. Monte-Carlo validation of PCE surrogate model for the five investigated data-sets. A total of 5000 model evaluations for distinct parameter vectors were compared with the PCE surrogate prediction. PC-GSA bounds were used. The x-axis denotes the RMSE of PCE cell voltage prediction compared with the electrochemical model, higher values indicate less accurate SA results. The highest average RMSE of 4 mV was found for the BEV distribution truck data-set. (For interpretation of the references to color in this figure legend, the reader is referred to the web version of this article.)

coefficients but to some degree observed in all sub-figures. This means that the importance of these parameters depends on their true values. For instance, the SEI layer thickness could, depending on the nominal value, have the largest impact of all parameters, or no impact at all. A large box signifies that the impact of a parameter is affected by the values of other parameters. This interaction is most noticeable for the volume fractions and the Bruggeman coefficients but cannot be quantified using this screening approach. This confirms that local derivative based or one-at-a-time approaches for sensitivity analysis significantly depend on constant assumed nominal values and the employed GSA approach is more suitable when little information about true parameter estimates is available.

5.2.3. Synthetic parametrization

The GSA performed up to this point indicated that driving data is useful to identify a large fraction of the investigated parameter set, especially when large SOC windows, high currents, and significant polarization is present in the vehicle data. The GSA is by definition only an average measure over the whole physics- or aging-constrained parameter ranges and sensitivities at the true value are not automatically equivalent to computed Sobol' indices. To validate the GSA we therefore performed a synthetic parameter estimation study. The *true* parameter vector was set and a synthetic truth was generated by the employed model. To mimic real-world identification, a normally distributed noise term with a 5 mV standard deviation and 0 V mean was added to the synthetic truth (Eq. (41)):

$$y_m = y(\boldsymbol{\theta}) + \upsilon \tag{41}$$

where y_m is the synthetic measured voltage and $\upsilon \sim \mathcal{N}(0, \sigma^2)$ the stochastic noise. This stochastic component leads to a unique estimate for every estimation study. To gain meaningful measures for parameter estimate confidence bounds under the prescribed noise conditions, we performed 100 parameter estimations on each data-set. The non-linear least-squares regression problem (Eq. (42))

$$\text{minimize} \quad \sum_{k=0}^{N} (y(k, \hat{\boldsymbol{\theta}}) - y_m(k))^2 \quad \text{subject to} \quad \boldsymbol{\theta}_l \leq \hat{\boldsymbol{\theta}} \leq \boldsymbol{\theta}_u \tag{42}$$

was solved using the derivative free solver developed by Cartis et al. [58] assuming aging constrained bounds $\boldsymbol{\theta}_{l,u}$ from Table 3. $\hat{\boldsymbol{\theta}}$ is the parameter estimate.

The resulting PDFs comparing the BEV and PHEV trucks as well as the slow charge data-sets are given in Fig. 11. The PDFs were computed using a kernel density estimation [59] and normalizing the results to have the same area. The BEV truck contains both a large utilized SOC window and large currents, while the other data-sets only contain one or the other. A narrow PDF means that the variance of the estimate is low and thus it's confidence high. Such was the case for e.g. the SEI layer thickness parameter in both the BEV and the PHEV truck. A wide PDF implies small confidence in the estimate. This was the case e.g. in the positive electrode solid diffusion time constant and in the separator Bruggeman coefficient. For these parameters, there was a significant bias between the most likely estimate and the true value that seems to be strongly influenced by the initial guess. In the case of volume fractions and Bruggeman coefficients in the electrodes, some symmetry in the PDFs and the second order interactions observed in Fig. 5 insinuates that parameters are not identifiable separately, and instead a combination should be estimated. We included these combinations (active material volume fractions and electrolyte tortuosities) in the last row of Fig. 11. This shows that the investigated synthetic data with the assumed true parameter vector does not cause sufficient concentration polarization in the electrolyte (Eq. 1), as this is the only equation that the porosity parameter appears independently and therefore uncoupled from its impact on capacity, tortuosity, and interfacial surface area.

The parameters that were deemed most important in the GSA mostly show narrow confidence bounds and small bias implying strong identifiability. The GSA predicted that the positive electrode diffusion time constant and the separator Bruggeman coefficient are not identifiable in any of the investigated data-sets which can be confirmed in this validation, as neither parameter can accurately be determined. For the negative electrode diffusion time constant the BEV truck data-set yielded an estimate with small bias. However, the confidence in the estimate is small as the PDF is wide. The current collector resistance in the positive electrode was deemed important in all data-sets except the slow charge by the GSA, however it could not be identified accurately. The true value for this parameter is near the lower bound where it's sensitivity is lowest as shown in the non-linearity analysis (Fig. 10). It therefore likely contributes only little to the cell voltage making it unidentifiable. If this resistance were to increase during battery aging it would become identifiable at some stage. This once again highlights how the GSA can only with certainty determine global unidentifiability while local identifiability must be confirmed a posteriori. Strong identifiability of bulked tortuosities and active material volume fractions confirms that even low levels of interaction as shown in Fig. 5 can insinuate practical unidentifiability. Residuals between synthetic truth and estimated states for the BEV truck are given in the supplementary material (Fig. A.2) and show that bias in individual parameters does not cause bias in state-estimation. It indicates that the bulked parameters are what is important also for state prediction.

6. Summary and conclusion

We demonstrated a methodology to guide electrochemical model-based battery management re-parametrization under real-world conditions. To this end, we studied global sensitivity measures of 14 Doyle–Fuller–Newman (DFN) model parameters to three representative real-world driving patterns and two charging protocols for heavy-duty vehicles.

The results were obtained assuming known aging-independent electrolyte properties, a given cell geometry and isothermal operation. Each set of simulations for the same data-set was initiated at the same cell voltage. Physics and aging-constrained bounds were set based on literature where possible. Aging-induced changes in model parameters are dependent on cell chemistry and utilization and cannot account

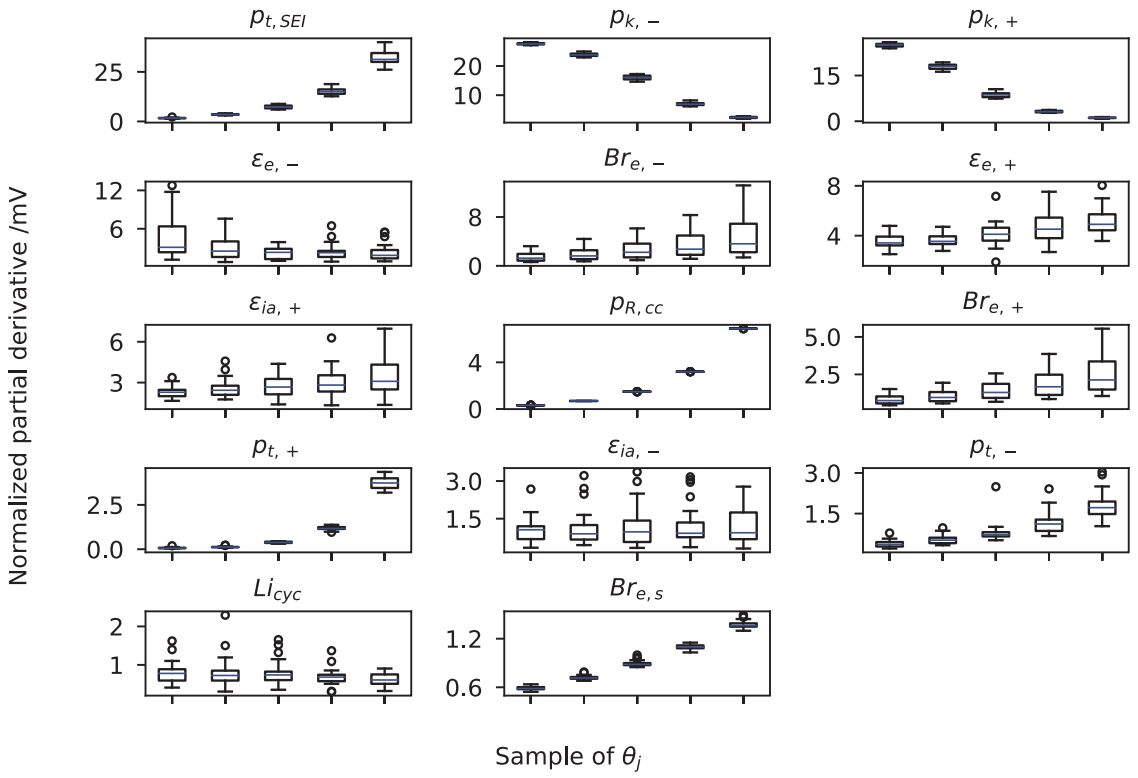

Fig. 10. Absolute value of the average normalized partial derivative throughout the BEV truck data-set for 5 evenly spread out values of θ_j and 30 different realizations of the other parameters. Circles represent outliers. The values 1 to 5 for each parameter represents 1/6th to 5/6th of the parameter interval specified in Table 3. Large deviations of computed sensitivities shown through both the σ and 2σ confidence intervals in the box plots show that parameter sensitivities depend on nominal values of other parameters. Significant changes in median value (blue lines) over the x-axis highlights the dependence of local sensitivity measures on their own nominal value.

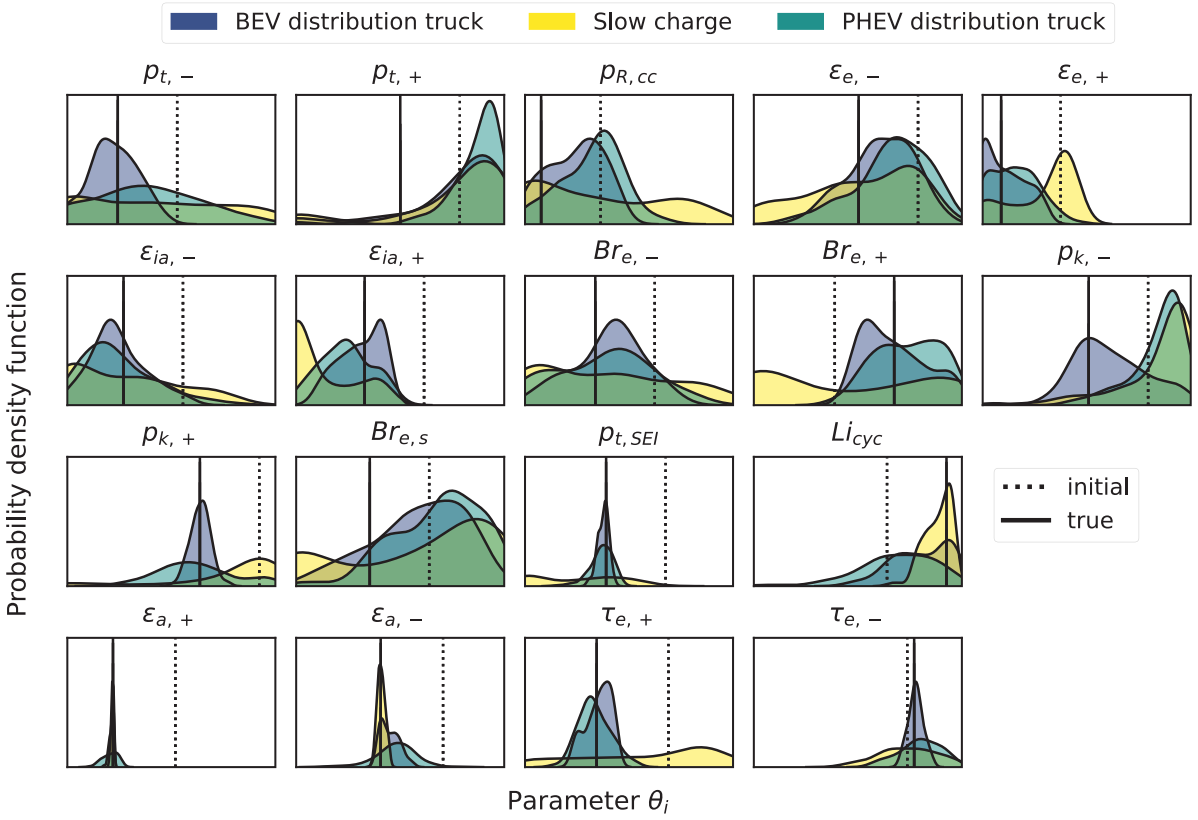

Fig. 11. Parameter PDFs of 100 parameter estimates for the BEV Truck data-set. Initial values were set at a 30% offset from the synthetic truth and are indicated with the dotted line. The x- and y-axes are normalized. The curves were computed with a kernel density estimation from the parameter histograms. The last row contains bulked parameters for active material volume fractions and tortuosities. (For interpretation of the references to color in this figure legend, the reader is referred to the web version of this article.)

for abusive usage. Furthermore, we set a high noise level to account for low measurement accuracy in vehicle instrumentation. Given these assumptions, we summarize our conclusions as follows:

- A global sensitivity analysis (GSA) with parameter spans motivated by physical feasibility showed that all studied parameters produced voltage variance above the sensitivity threshold 2.5×10^{-5} V^2 for one or several of the vehicle driving data sets. To reliably model cells in heavy-duty vehicle applications, none of the studied parameter values can be assumed but must be assigned through some identification scheme. Furthermore, a majority of the parameters are on average excited by the driving data which enables full or partial model parametrization without any additional instrumentation or experimentation.
- We investigated three vehicle types with distinct usage patterns and showed that parameter sensitivity depends strongly on vehicle use. In general, higher currents, larger SOC windows, and increased polarization increase sensitivity. Thus, the necessary re-parametrization is different depending on the characteristic usage of a vehicle battery system. The BEV truck requires re-parametrization of 9 parameters whereas a model in the PHEV truck could maintain predictive performance by updating only 4 ohmic/kinetic parameters.
- Important states like electrode concentrations and lithium plating potential are sensitive to changes of the SEI thickness, volume fractions and reaction rates. We observed that parameters important for internal states are also sensitive to cell voltage, which means re-parametrization from input–output data measured onboard is enabled. This is an important conclusion that supports the viability of an electrochemical BMS since e.g. control of lithium plating rate could be maintained in an aging battery.
- Low global sensitivity and/or high interaction effect correlated with low estimation accuracy in a synthetic parametrization study. We showed that interaction quantified in the GSA predicts which interaction must be de-coupled by bulking parameters for a unique and accurate parametrization. This was the case for active material volume fractions and electrolyte tortuosities.

Finally, we provide a comparison with previous works focusing on passenger car driving. The comparison is qualitative due to the different input data, parameter sets, and assumptions used: both Li et al. [24] and Gao et al. [25] conclude that capacity parameters are essential to update at full (Gao et al. and Li et al.) or partial (Li et al.) SOC windows. We show how partial SOC windows present in some heavy-duty vehicle applications do not excite capacity parameters sufficiently. We confirm that the C-rate is crucial for remaining dynamic parameters however, while Li et al. show low sensitivity of electrolyte parameters, we highlight how tortuosity plays an important role in energy-optimized heavy-duty vehicle batteries. Previous works do not account for parameter interactions and the proposed link between parameter sensitivity and identifiability is therefore not complete. We quantify parameter interaction and demonstrate how this information is practical for obtaining a unique parametrization. Li et al. conducted a one-at-a-time local SA [24] and concluded that parameters important for state prediction also are sensitive to cell voltage, which we confirm with our global study.

To summarize, global sensitivity analysis shows which parameters are important to re-parametrize in an electrochemical BMS and indicates which parameters are identifiable during characteristic vehicle usage. Ultimately, we show that there is significant potential in adapting electrochemical BMS to use cases and a need to tailor re-parametrization strategy to the application to achieve unique parametrization and accurate control.

Abbreviations

See Table 6

Table 6
List of abbreviations.

Abbreviation	Full text
AC - GSA	aging constrained global sensitivity analysis
BEV	battery electric vehicle
BMS	battery management system
BOL	beginning-of-life
CC	current collector
DFN	Doyle–Fuller–Newman
GSA	global sensitivity analysis
LHS	latin-hypercube-sampling
OCP	open circuit potential
PCE	polynomial chaos expansion
PC - GSA	physics-constrained global sensitivity analysis
PDF	probability densitiy function
PHEV	plug-in hybrid electric vehicle
RMSE	root-mean-square error
SA	sensitivity analysis
SEI	solid electrolyte-interphase
SOC	state-of-charge
SOH	state-of-health

CRediT authorship contribution statement

Moritz Streb: Conceptualization, Formal analysis, Investigation, Data curation, Writing – original draft, Writing – review & editing, Visualization. **Malin Andersson:** Conceptualization, Formal analysis, Investigation, Data curation, Writing – original draft, Writing – review & editing, Visualization. **Verena Löfqvist Klass:** Writing – review & editing, Supervision, Funding acquisition. **Matilda Klett:** Writing – review & editing, Supervision, Funding acquisition. **Mikael Johansson:** Writing – review & editing, Supervision, Funding acquisition. **Göran Lindbergh:** Writing – review & editing, Supervision, Funding acquisition.

Declaration of competing interest

The authors declare that they have no known competing financial interests or personal relationships that could have appeared to influence the work reported in this paper.

Data availability

The data that has been used is confidential.

Acknowledgments

This work was funded by the Swedish Electromobility Center and Swedish Energy Agency through the FFI program Energy and Environment (project number 47103-1).

Appendix A. Supplementary data

Supplementary material related to this article can be found online at https://doi.org/10.1016/j.etran.2023.100231.

References

[1] Zhang R, Fujimori S. The role of transport electrification in global climate change mitigation scenarios. Environ Res Lett 2020;15(3):034019. http://dx.doi.org/10.1088/1748-9326/ab6658.

[2] Han X, Lu L, Zheng Y, Feng X, Li Z, Li J, et al. A review on the key issues of the lithium ion battery degradation among the whole life cycle. ETransportation 2019;1:100005. http://dx.doi.org/10.1016/j.etran.2019.100005.

[3] Forrest K, Mac Kinnon M, Tarroja B, Samuelsen S. Estimating the technical feasibility of fuel cell and battery electric vehicles for the medium and heavy duty sectors in California. Appl Energy 2020;276:115439. http://dx.doi.org/10.1016/j.apenergy.2020.115439.

[4] Dai H, Jiang B, Hu X, Lin X, Wei X, Pecht M. Advanced battery management strategies for a sustainable energy future: Multilayer design concepts and research trends. Renew Sustain Energy Rev 2021;138:25. http://dx.doi.org/10.1016/j.rser.2020.110480.

[5] Li W, Demir I, Cao D, Jöst D, Ringbeck F, Junker M, et al. Data-driven systematic parameter identification of an electrochemical model for lithium-ion batteries with artificial intelligence. Energy Storage Mater 2022;44:557–70. http://dx.doi.org/10.1016/j.ensm.2021.10.023.

[6] Wang Y, Tian J, Sun Z, Wang L, Xu R, Li M, et al. A comprehensive review of battery modeling and state estimation approaches for advanced battery management systems. Renew Sustain Energy Rev 2020;131:110015. http://dx.doi.org/10.1016/j.rser.2020.110015.

[7] Yang S, Zhang C, Jiang J, Zhang W, Zhang L, Wang Y. Review on state-of-health of lithium-ion batteries: Characterizations, estimations and applications. J Clean Prod 2021;314:128015. http://dx.doi.org/10.1016/j.jclepro.2021.128015.

[8] Bi Y, Yin Y, Choe S-Y. Online state of health and aging parameter estimation using a physics-based life model with a particle filter. J Power Sources 2020;476:228655. http://dx.doi.org/10.1016/j.jpowsour.2020.228655.

[9] Mayilvahanan KS, Soni JR, Takeuchi KJ, Takeuchi ES, Marschilok AC, West AC. Parameter estimation for electrode degradation: Learning in the face of model-experiment discrepancies. J Electrochem Soc 2022;169(5):050517. http://dx.doi.org/10.1149/1945-7111/ac6c0e.

[10] Ye M, Hill M. Chapter 10 - global sensitivity analysis for uncertain parameters, models, and scenarios. In: Petropoulos GP, Srivastava PK, editors. Sensitivity analysis in earth observation modelling. Elsevier; 2017, p. 177–210. http://dx.doi.org/10.1016/B978-0-12-803011-0.00010-0.

[11] Smith KA. Electrochemical control of lithium-ion batteries. IEEE Control Syst Mag 2010;30(2):18–25. http://dx.doi.org/10.1109/MCS.2010.935882.

[12] Perez H, Shahmohammadhamedani N, Moura S. Enhanced performance of Li-ion batteries via modified reference governors and electrochemical models. IEEE/ASME Trans Mechatronics 2015;20(4):1511–20. http://dx.doi.org/10.1109/TMECH.2014.2379695.

[13] Tulsyan A, Tsai Y, Gopaluni RB, Braatz RD. State-of-charge estimation in lithium-ion batteries: A particle filter approach. J Power Sources 2016;331:208–23. http://dx.doi.org/10.1016/j.jpowsour.2016.08.113.

[14] Namor E, Sossan F, Torregrossa D, Cherkaoui R, Paolone M. Battery storage system optimal exploitation through physics-based model predictive control. In: 2017 IEEE manchester powertech. IEEE; 2017, p. 1–6. http://dx.doi.org/10.1109/PTC.2017.7981145.

[15] Florentino G, Trimboli MS. Lithium-ion battery management using physics-based model predictive control and DC-DC converters. In: 2018 IEEE transportation electrification conference and expo. IEEE; 2018, p. 916–21. http://dx.doi.org/10.1109/ITEC.2018.8450187.

[16] Li Y, Vilathgamuwa M, Wikner E, Wei Z, Zhang X, Thiringer T, et al. Electrochemical model-based fast charging: Physical constraint-triggered PI control. IEEE Trans Energy Convers 2021. http://dx.doi.org/10.1109/TEC.2021.3065983.

[17] Pozzi A, Raimondo DM. Stochastic model predictive control for optimal charging of electric vehicles battery packs. J Energy Storage 2022;55:105332. http://dx.doi.org/10.1016/j.est.2022.105332.

[18] Andersson M, Streb M, Ko JY, Klass VL, Klett M, Ekström H, et al. Parametrization of physics-based battery models from input–output data: A review of methodology and current research. J Power Sources 2022;521:230859. http://dx.doi.org/10.1016/j.jpowsour.2021.230859.

[19] Yang X-G, Leng Y, Zhang G, Ge S, Wang C-Y. Modeling of lithium plating induced aging of lithium-ion batteries: Transition from linear to nonlinear aging. J Power Sources 2017;360:28–40. http://dx.doi.org/10.1016/j.jpowsour.2017.05.110.

[20] Ekström H, Lindbergh G. A model for predicting capacity fade due to SEI formation in a commercial graphite/LiFePO $_4$ cell. J Electrochem Soc 2015;162(6):A1003–7. http://dx.doi.org/10.1149/2.0641506jes.

[21] Vetter J, Novák P, Wagner MR, Veit C, Möller KC, Besenhard JO, et al. Ageing mechanisms in lithium-ion batteries. J Power Sources 2005;147(1–2):269–81. http://dx.doi.org/10.1016/j.jpowsour.2005.01.006.

[22] Wei Z, Zou C, Leng F, Soong BH, Tseng K-J. Online model identification and state-of-charge estimate for lithium-ion battery with a recursive total least squares-based observer. IEEE Trans Ind Electron 2018;65(2):1336–46. http://dx.doi.org/10.1109/TIE.2017.2736480.

[23] Andersson M, Johansson M, Klass Löfqvist V. A continuous-time LPV model for battery state-of-health estimation using real vehicle data. In: 2020 IEEE conference on control technology and applications. IEEE; 2020, p. 692–8. http://dx.doi.org/10.1109/CCTA41146.2020.9206257.

[24] Li W, Cao D, Jöst D, Ringbeck F, Kuipers M, Frie F, et al. Parameter sensitivity analysis of electrochemical model-based battery management systems for lithium-ion batteries. Appl Energy 2020;269:115104. http://dx.doi.org/10.1016/j.apenergy.2020.115104.

[25] Gao Y, Zhang X, Zhu C, Guo B. Global parameter sensitivity analysis of electrochemical model for lithium-ion batteries considering aging. IEEE/ASME Trans Mechatronics 2021;26(3):1283–94. http://dx.doi.org/10.1109/TMECH.2021.3067923.

[26] Doyle M, Fuller TF, Newman J. Modelling of the galvanostatic charge and discharge of the lithium/polymer/insertion cell. J Electrochem Soc 1993;140(6):1526–33. http://dx.doi.org/10.1149/1.2221597.

[27] Lin N, Xie X, Schenkendorf R, Krewer U. Efficient global sensitivity analysis of 3D multiphysics model for Li-ion batteries. J Electrochem Soc 2018;165(7):A1169. http://dx.doi.org/10.1149/2.1301805jes.

[28] Saltelli A, Annoni P. How to avoid a perfunctory sensitivity analysis. Environ Model Softw 2010;25(12):1508–17. http://dx.doi.org/10.1016/j.envsoft.2010.04.012.

[29] Saltelli A, Aleksankina K, Becker W, Fennell P, Ferretti F, Holst N, et al. Why so many published sensitivity analyses are false: A systematic review of sensitivity analysis practices. Environ Model Softw 2019;114:29–39. http://dx.doi.org/10.1016/j.envsoft.2019.01.012.

[30] Fan C, Grandjean TR, O'Regan K, Kendrick E, Widanage WD. Understanding non-linearity in electrochemical systems using multisine-based non-linear characterization. Trans Inst Meas Control 2021. http://dx.doi.org/10.1177/01423312211045991.

[31] Khalik Z, Donkers MCF, Sturm J, Bergveld HJ. Parameter estimation of the Doyle–Fuller–Newman model for Lithium-ion batteries by parameter normalization, grouping, and sensitivity analysis. J Power Sources 2021;499:229901. http://dx.doi.org/10.1016/j.jpowsour.2021.229901.

[32] Wang AA, O'Kane SEJ, Brosa Planella F, Houx JL, O'Regan K, Zyskin M, Edge J, Monroe CW, Cooper SJ, Howey DA, Kendrick E, Foster JM. Review of parameterisation and a novel database (LiionDB) for continuum Li-ion battery models. Progress in Energy 2022;4(3):032004. http://dx.doi.org/10.1088/2516-1083/ac692c.

[33] Sulzer V, Marquis SG, Timms R, Robinson M, Chapman SJ. Python battery mathematical modelling (PyBaMM). J Open Res Softw 2021;9:14. http://dx.doi.org/10.5334/jors.309.

[34] Landesfeind J, Gasteiger HA. Temperature and concentration dependence of the ionic transport properties of lithium-ion battery electrolytes. J Electrochem Soc 2019;166(14):A3079–97. http://dx.doi.org/10.1149/2.0571912jes.

[35] Forman JC, Moura SJ, Stein JL, Fathy HK. Genetic identification and fisher identifiability analysis of the Doyle–Fuller–Newman model from experimental cycling of a LiFePO4 cell. J Power Sources 2012;210:263–75. http://dx.doi.org/10.1016/j.jpowsour.2012.03.009.

[36] Safari M, Morcrette M, Teyssot A, Delacourt C. Multimodal physics-based aging model for life prediction of Li-ion batteries. J Electrochem Soc 2009;156(3):A145. http://dx.doi.org/10.1149/1.3043429.

[37] Mohtat P, Lee S, Sulzer V, Siegel JB, Stefanopoulou AG. Differential expansion and voltage model for Li-ion batteries at practical charging rates. J Electrochem Soc 2020;167(11):110561. http://dx.doi.org/10.1149/1945-7111/aba5d1.

[38] Ramadesigan V, Chen K, Burns NA, Boovaragavan V, Braatz RD, Subramanian VR. Parameter estimation and capacity fade analysis of lithium-ion batteries using reformulated models. J Electrochem Soc 2011;158(9):A1048. http://dx.doi.org/10.1149/1.3609926.

[39] Lee JT, Nitta N, Benson J, Magasinski A, Fuller TF, Yushin G. Comparative study of the solid electrolyte interphase on graphite in full Li-ion battery cells using X-ray photoelectron spectroscopy, secondary ion mass spectrometry, and electron microscopy. Carbon 2013;52:388–97. http://dx.doi.org/10.1016/j.carbon.2012.09.049.

[40] Yoshida T, Takahashi M, Morikawa S, Ihara C, Katsukawa H, Shiratsuchi T, et al. Degradation mechanism and life prediction of lithium-ion batteries. J Electrochem Soc 2006;153(3):A576. http://dx.doi.org/10.1149/1.2162467.

[41] Zhou X, Pan Z, Han X, Lu L, Ouyang M. An easy-to-implement multi-point impedance technique for monitoring aging of lithium ion batteries. J Power Sources 2019;417:188–92. http://dx.doi.org/10.1016/j.jpowsour.2018.11.087.

[42] Yang X-G, Leng Y, Zhang G, Ge S, Wang C-Y. Modeling of lithium plating induced aging of lithium-ion batteries: Transition from linear to nonlinear aging. J Power Sources 2017;360:28–40. http://dx.doi.org/10.1016/j.jpowsour.2017.05.110.

[43] Ge H, Aoki T, Ikeda N, Suga S, Isobe T, Li Z, et al. Investigating lithium plating in lithium-ion batteries at low temperatures using electrochemical model with NMR assisted parameterization. J Electrochem Soc 2017;164(6):A1050. http://dx.doi.org/10.1149/2.0461706jes.

[44] Colclasure AM, Tanim TR, Jansen AN, Trask SE, Dunlop AR, Polzin BJ, et al. Electrode scale and electrolyte transport effects on extreme fast charging of lithium-ion cells. Electrochim Acta 2020;337:135854. http://dx.doi.org/10.1016/j.electacta.2020.135854.

[45] Schweidler S, de Biasi L, Schiele A, Hartmann P, Brezesinski T, Janek J. Volume changes of graphite anodes revisited: a combined operando X-ray diffraction and in situ pressure analysis study. J Phys Chem C 2018;122(16):8829–35. http://dx.doi.org/10.1021/acs.jpcc.8b01873.

[46] Ruan Y, Song X, Fu Y, Song C, Battaglia V. Structural evolution and capacity degradation mechanism of LiNi0.6Mn0.2Co0.2O2 cathode materials. J Power Sources 2018;400:539–48. http://dx.doi.org/10.1016/j.jpowsour.2018.08.056.

[47] Valøen LO, Reimers JN. Transport properties of LiPF6-based Li-ion battery electrolytes. J Electrochem Soc 2005;152(5):A882. http://dx.doi.org/10.1149/1.1872737.

[48] Figueiredo MA, Dias JB, Oliveira JP, Nowak RD. On total variation denoising: A new majorization-minimization algorithm and an experimental comparisonwith wavalet denoising. In: 2006 International conference on image processing. IEEE; 2006, p. 2633–6. http://dx.doi.org/10.1109/ICIP.2006.313050.

[49] Sobol IM. Sensitivity analysis for non-linear mathematical models. Math Model Comput Exp 1993;1:407–14.
[50] Dobre S, Bastogne T, Profeta C, Barberi-Heyob M, Richard A. Limits of variance-based sensitivity analysis for non-identifiability testing in high dimensional dynamic models. Automatica 2012;48(11):2740–9. http://dx.doi.org/10.1016/j.automatica.2012.05.004.
[51] Saltelli A. Global sensitivity analysis: An introduction. In: Proceedings of the 4th international conference on sensitivity analysis of model output. 2004.
[52] Saltelli A, Ratto M, Andres T, Campolongo F, Cariboni J, Gatelli D, et al. Global sensitivity analysis. The primer. John Wiley & Sons, Ltd; 2007, http://dx.doi.org/10.1002/9780470725184.
[53] Crestaux T, Le Maître O, Martinez J-M. Polynomial chaos expansion for sensitivity analysis. Reliab Eng Syst Saf 2009;94(7):1161–72. http://dx.doi.org/10.1016/j.ress.2008.10.008, Special Issue on Sensitivity Analysis.
[54] Weise K, Poßner L, Müller E, Gast R, Knösche TR. Pygpc: A sensitivity and uncertainty analysis toolbox for Python. SoftwareX 2020;11:100450. http://dx.doi.org/10.1016/j.softx.2020.100450.
[55] Helton JC, Davis F, Johnson JD. A comparison of uncertainty and sensitivity analysis results obtained with random and Latin hypercube sampling. Reliab Eng Syst Saf 2005;89(3):305–30. http://dx.doi.org/10.1016/j.ress.2004.09.006.
[56] Guillaume JH, Jakeman JD, Marsili-Libelli S, Asher M, Brunner P, Croke B, et al. Introductory overview of identifiability analysis: A guide to evaluating whether you have the right type of data for your modeling purpose. Environ Model Softw 2019;119:418–32. http://dx.doi.org/10.1016/j.envsoft.2019.07.007.
[57] Ghasemizade M, Baroni G, Abbaspour K, Schirmer M. Combined analysis of time-varying sensitivity and identifiability indices to diagnose the response of a complex environmental model. Environ Model Softw 2017;88:22–34. http://dx.doi.org/10.1016/j.envsoft.2016.10.011.
[58] Cartis C, Fiala J, Marteau B, Roberts L. Improving the flexibility and robustness of model-based derivative-free optimization solvers. ACM Trans Math Softw 2019;45(3):1–41. http://dx.doi.org/10.1145/3338517.
[59] Virtanen P, Gommers R, Oliphant TE, Haberland M, Reddy T, Cournapeau D, et al. SciPy 1.0: Fundamental Algorithms for Scientific Computing in Python. Nature Methods 2020;17:261–72. http://dx.doi.org/10.1038/s41592-019-0686-2.